# Spin-On Catalyst: Straightforward and Flexible Route to Substrate-Grown Single Wall Carbon Nanotubes

Mark J. Pender,† Laura A. Sowards, Benji Maruyama, Richard A. Vaia, and Morley O. Stone*

*Materials and Manufacturing Directorate, Air Force Research Laboratory, 3005 Hobson Way, Wright-Patterson Air Force Base, Ohio 45433-7702*

*Received September 12, 2003. Revised Manuscript Received January 28, 2004*

The synthesis and characterization of single-wall carbon nanotubes (SWNTs) from simple catalytic precursors at 900 °C from methane and hydrogen is demonstrated. The catalyst precursor is comprised of iron nitrate and a commercially available siloxane polymer solution and is applied to various substrates via spin coating or dipping. The siloxane matrix simultaneously provides for the controlled formation of catalytic nanoparticles via phase separation and, upon heating, a smooth, continuous film of $SiO_x$, which prevents catalyst coarsening and agglomeration at growth conditions. Furthermore, the processibility of the polymer enables the formation of complex, 3D structures from which nanotubes can grow. This combination of processing ease, flexibility, and inherent multifunctionality provides facile, controllable growth of single-wall carbon nanotubes on a multitude of substrates and facilitates additional routes toward SWNT-based device fabrication.

## Introduction

Carbon nanotubes (CNTs), both multiwall and single wall, are proving to be critical components for emerging electronic, sensor, and structural systems.[1] In many instances, the key to success is the development of synthetic routes compatible with manufacturing and application requirements (volume, perfection, order, arrangement, etc.). For the construction of single-wall nanotube (SWNT) devices, spatial and orientational control is necessary. This control may be obtained by either well-defined placement and orientation of nanotubes isolated from bulk growth methods or by direct growth of single-wall nanotubes from the area of interest. The latter route is highly promising when considering that defined tube orientation may be obtained using an external bias, such as a local electric field,[2] crystallographic orientation of the underlying substrate,[3] or gas flow.[4] For example, Liu and co-workers recently demonstrated the construction of orthogonal networks of millimeter-long SWNTs by a method in which the direction of gas flow led to oriented growth.[4] Intricate work has also demonstrated complex structure formation in the growth of suspended SWNTs between silicon pillars.[5]

For the successful integration of nanotubes into devices by a direct growth method, several technical issues must be addressed. These include control of catalyst particle density, reactivity, location, and size (with respect to both the as-synthesized diameter and the prevention of high-temperature coarsening and agglomeration), as well as complete elucidation of the reaction parameters for efficient SWNT nucleation and growth, thereby providing prescribed orientation, size (diameter and length), and, perhaps, type (n,m indices) of nanotubes. Much work has been done to effectively control the size of nanotube catalysts, and subsequently the nanotube diameter, but often the approaches are expensive or laborious.[6] For example, sputtering of thin catalytic films on substrates[7] has proven successful in some cases, but often requires the use of an interlayer, such as thermally grown silicon oxide, alumina,[8a] or magnesium[8b] oxide. Comparable to powders and con-

* To whom correspondence should be addressed. E-mail: morley.stone@wpafb.af.mil. Tel: 937-255-3808, ext 3180.

† National Research Council associate.

(1) For recent reviews see (a) Maruyama, B.; Alam, K. *SAMPE* **2002**, *38* (3), 59−70. (b) Thostenson, E. T.; Zhifeng, R.; Chou, T. W. *Comput. Sci. Technol.* **2001**, *6*, 1899−1912. (c) Harris, P. J. *Carbon Nanotubes and Related Structures: New Materials for the Twenty-First Century;* Cambridge University Press: New York, 1999. (d) Avouris, P. *Acc. Chem. Res.* **2002**, *35* (12), 1026−1034. (e) Dai, H. *Acc. Chem. Res.* **2002**, *35* (12), 1035−1044.

(2) (a) Joselevich, E.; Lieber, C. M. *Nano Lett.* **2002**, *2* (10), 1137−1141. (b) Zhang, Y.; Chan, A.; Cao, J.; Wang, Q.; Kim, W.; Li, Y.; Morris, N.; Yenilmez, E.; Kong, J.; Dai, H. *Appl. Phys. Lett.* **2001**, *79*, 3155−3157.

(3) Su, M.; Li, Y.; Maynor, B.; Buldum, A.; Lu, J. P.; Liu, J. *J. Phys. Chem. B* **2000**, *104* (28), 6505−6508.

(4) Huang, S.; Cai, X.; Liu, J. *J. Am. Chem. Soc.* **2003**, *125*, 5636−5637.

(5) (a) Franklin, N. R.; Dai, H. *Adv. Mater.* **2000**, *12* (12), 890−894. (b) Homma, Y.; Kobayashi, Y.; Ogino, T.; Yamashita, T. *Appl. Phys. Lett.* **2002**, *81* (12), 2261−2263.

(6) For example (a) Li, Y.; Woong, K.; Zhang, Y.; Rolandi, M.; Wang, D.; Dai, H. *J. Phys. Chem. B* **2001**, *105*, 11424−11431. (b) An, L.; Owens, J. M.; McNeil, L. E.; Liu, J. *J. Am. Chem. Soc.* **2002**, *124* (46), 13688−13689.

(7) For example (a) Zhang, R. Y.; Amlani, I.; Baker, J.; Tresek, J.; Tsui, R. K.; Fejes, P. *Nano Lett.* **2003**, *3* (6), 731−735. (b) Hongo, H.; Yudasaka, M.; Ichihashi, T.; Nihey, F.; Iijima, S. *Chem. Phys. Lett.* **2002**, *361*, 349−354. (c) Nerushev, O. A.; Morjan, R.-E.; Ostrovskii, D. I.; Sveningsson, M.; Jönsson, M.; Rohmund, F.; Campbell, E. E. B. *Physica B* **2002**, *323*, 51−59. (d) Yoon, Y. J.; Bae, J. C.; Baik, H. K.; Cho, S. J.; Lee, S.-J.; Song, K. M.; Myung, N. S. *Physica B* **2002**, *323*, 318−320.

(8) For example (a) Delzeit, L.; Chen, B.; Cassell, A.; Stevens, R.; Nguyen, C.; Meyyappan, M. *Chem. Phys. Lett.* **2001**, *348*, 368−374. (b) Li, Q.; Hao, Y.; Li, X.; Zhang, J.; Liu, Z. *Chem. Mater.* **2002**, *14* (10), 4262−4266.

10.1021/cm034851s CCC: $27.50 
Published on Web 05/27/2004

densation-derived oxide films doped with catalytic metals,[9] substrate−catalyst interaction may be optimized to prevent catalyst agglomeration but not inhibit SWNT growth. However, these approaches can lead to rough surfaces, incompatible materials, and substantial amorphous carbon deposition during nanotube growth—all of which are unsuitable for microelectronic devices.

Recently, a material blend concept, consisting of a solution of poly(ethylene glycol), magnesium nitrite, and iron nitrate,[8b] was demonstrated as a flexible route to substrate growth of SWNTs. The polymer functioned as a delivery agent as well as a mediator for the formation of a catalytic substrate. During decomposition and volatilization (600 °C in air) of the polymer film, islands of MgO impregnated with iron oxide nanoparticles formed, which served as the catalytic sites for SWNT growth. Attractive for its simplicity, the resultant, discontinuous, rough films and the requirement of an intermediate, high-temperature oxidation step are detrimental for various device components and minimize the number of viable substrates.

Herein, a preceramic polymer−metal salt blend is demonstrated as a viable matrix for single-wall carbon nanotube catalysts. In contrast to the use of a sacrificial polymer, a preceramic polymer will not only mediate the formation of metallic catalysts suitable for SWNT growth, but also has the inherent property of directly transforming to a smooth, continuous substrate film without the requirement of an intermediate, high-temperature oxidation step. This enhances the options for the construction of SWNT-based devices by direct growth of nanotubes.

## Experimental Section

Catalytic coatings, referred to as spin-on catalyst (SOC#, where # is mg/mL concentration of iron nitrate), were formed by spin-coating a mixture of iron nitrate and Accu-glass T1-11 (Honeywell Electronics) onto an as-received silicon wafer (111; TTI Silicon) at 2000 rpm, yielding films ∼150 nm thick. After application, the coated substrate was subjected to typical CCVD conditions required for nanotube growth.[6a] Specifically, the coated wafer was transferred to a tube furnace, which was purged with nitrogen. The system was then ramped to 900 °C at 10°/min under $N_2$ and allowed to equilibrate for 10 min. The inert environment was exchanged with a mixture of flowing $CH_4$ and $H_2$ at 350 sccm each. After 15 min, the reactive atmosphere was replaced with $N_2$ and the coated wafer was allowed to cool under the $N_2$ flow. The final $SiO_x$ films were ∼100 nm thick. Rutherford backscattering indicated that the compositional distribution of Fe normal to the film surface before and after thermal treatment was uniform.

Fibrils of SOC were formed by first allowing the solvent from a drop of the SOC4 solution to partially evaporate. Once the mixture was sufficiently viscous, a fiber was manually pulled from the mixture with a pair of tweezers. The fiber was then annealed in air to 180 °C for 2 h. After this treatment, the SOC4 fibril was placed in a tube furnace and subjected to the typical growth conditions.

For high-resolution transmission electron microscopy (HR-TEM) studies, gold TEM grids were immersed in a solution of SOC4 and dried under ambient conditions. The grids were then placed on a silicon wafer and subjected to the same growth conditions as previously described. Such experiments allowed analysis of the final products without scraping, sonication, or digestion of support materials by acid treatments. HRTEM images were obtained on a Philips CM200 at 200 kV. Atomic force microscopy (AFM) images were collected in Tapping Mode on a Digital Instruments Nanoscope IIIa multimode scanning probe microscope with a scan rate of 1 Hz. SEM images were obtained without a conductive coating on a Hitachi S5200 or an FEI XL30. Raman data were collected on a Renishaw inVia Raman microscope with ∼3 mW power at the sample.

Conductivity measurements were performed using a four-point probe geometry, at room temperature, and with currents from 1 to 100 nA. The sample configuration consisted of two parallel sets of leads stretched across a rectangular sample, were the separation between leads was much greater than the sample thickness ($SiO_x$ + SWNTs). Assuming the electric field is uniform and parallel within the sample given the electrode configuration, the conductivity of an isotropic material is $\sigma = (1/R)(L/A)$, where $R$ is the resistance, $L$ is the length over which the voltage drop is measured, and $A$ is the cross sectional area of the current density ($A = WT$, where $W$ is width and $T$ is thickness (SWNT network)). The surface resistivity (sheet resistance) is similarly defined as $R_S = R(W/L)$, with units of Ω/□ (ohms per square). Microscopy indicated that, on the dimensions of the electrode separation, the nanotubes were randomly oriented and uniformly distributed on the surface. The voltage leads were separated from the current leads to remove any contact resistance-derived voltage drop. Current was sourced (Keithley 220) at the outer pair of contacts while the voltage was measured at the inner pair of contacts utilizing a high input impedance electrometer (Keithley 617).

## Results

Figure 1 demonstrates the typical SWNT products grown at 900 °C in methane and hydrogen from various concentrations of iron nitrate in Accuglass T1-11 on silicon wafers. Accu-glass T1-11 is a methylsiloxane polymer solution used as a precursor to thin $SiO_x$ films for planarization in the microelectronics industry. It is a member of a broader family of preceramic polymers (silicates, phosphosilicates, and siloxanes) commonly referred to as spin-on glass (SOG). The film thickness of these samples ($SiO_x$ + SWNTs) is ∼100 nm. The thickness may be varied by spin speed and the coatings may be applied to any substrate that is stable and inert under the growth conditions (e.g., graphitic carbon and quartz).

Table 1 summarizes the characteristics of the particles and carbon nanotubes formed on the film surface with increasing iron nitrate concentration in the preceramic polymer. Note that edge-effect charging at the nanotube−$SiO_x$ interface distorts (increases) the apparent diameter of the nanotubes in the SEM images. Electron microscopy of nanotubes protruding off the surface (e.g., Figure 1e) or AFM images (e.g., Figure 1c) provide a better indication of the true diameter of the nanotubes. At the higher iron nitrate concentrations, surface roughness and inhomogeneities inhibited precise dimensional measurements by AFM—thus, values reported are a statistical average of at least 30 measurements.

Low concentrations of iron nitrate (0.05−0.5 mg/mL; Figure 1a and b) gave rise to particles, ∼5 nm in diameter, whose density increased with concentration.

(9) For example (a) Huang, L.; Wind, S. J.; O'Brien, S. P. *Nano Lett.* **2003**, *3* (3), 299−303. (b) Cassell, A. M.; Franklin, N. R.; Tombler, T. W.; Chan, E. M.; Han, J.; Dai, H. J. *J. Am. Chem. Soc.* **1999**, *121*, 7975. (c) Harutyunyan, A. R.; Pradhan, B. K.; Kim, U. J.; Chen, G. G.; Eklund, P. C. *Nano Lett.* **2002**, *2*, 525. (d) Li, Y. M.; Kim, W.; Zhang, Y. G.; Rolandi, M.; Wang, D. W.; Dai, H. J. *J. Phys. Chem. B* **2001**, *105*, 11424. (e) Fan, S.; Chapline, M. G.; Franklin, N. R.; Tombler, T. W.; Cassell, A. M.; Dai, H. *Science* **1999**, *283*, 512. (f) Hafner, J. H.; Bronikowski, M. J.; Azamian, B. R.; Nikolaev, P.; Rinzler, A. G.; Colbert, D. T.; Smith, K. A.; Smalley, R. E. *Chem. Phys. Lett.* **1998**, *296*, 195−202.

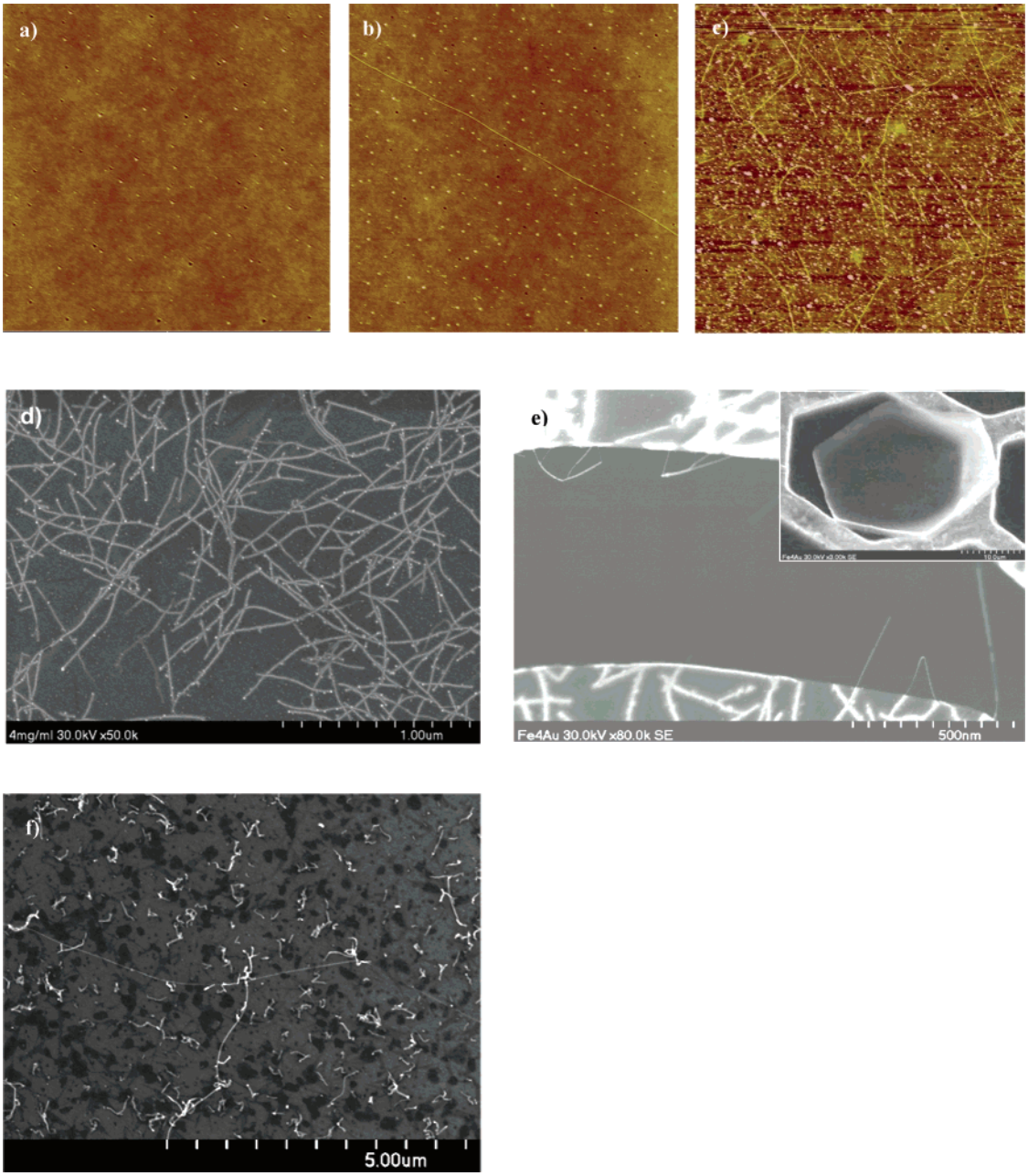


**Figure 1.** (a) Atomic force microscopy (AFM) image, 5-$\mu$m scan, of SOC0.05 film after growth with a surface roughness of ~2 Å. No nanotube growth was observed. (b) AFM image, 5- $\mu$m scan, of SOC0.5 film after growth showing a single nanotube on the surface. (c) AFM image, 5-$\mu$m scan, of SOC4 film after growth showing various individual carbon nanotubes. (d) Scanning electron microscopy (SEM) image of SOC4-derived carbon nanotubes. SEM images were obtained without a conductive coating. (e) SEM image of nanotubes grown from a SOC4-coated TEM grid. The inset shows a 30-$\mu$m hexagon of $SiO_x$ that has separated from the framework of the TEM grid and is coated on both sides with carbon nanotubes. (f) SEM image of SOC10 film after growth revealing a variety of carbon nanotube structures. In all images, growth conditions were 900 °C, 15 min, 350 sccm methane, and 350 sccm hydrogen.

**Table 1. Summary of the Characteristics of the Particles and Carbon Nanotubes Formed on the Film Surface with Increasing Iron Nitrate Concentration in the Preceramic Polymer**

| AFM data summary | SOC0.05 | SOC0.5 | SOC4.0 | SOC10 |
|---|---|---|---|---|
| tube height range (nm) | N/A | 0.5−3.2 | 0.5−4.2 | 8−36 |
| avg. height (SD) | | 1.32 (±0.70)[a] | 1.88 (±0.70) | 17.0 (±7.30)[a,b] |
| tube length ($\mu$m) | N/A | 5−30 | ? | 0.15−1.5 |
| est. particle diameter[c] (nm) | 5.40 (±2.02)[a] | 5.24 (±2.58) | 14.8 (±11.5) | 18.1 (±7.38)[a] |

[a] Averaged over smaller populations (<30). [b] Tubes with SWNT dimensions not included. [c] Measured height of particle assumed to be radius.

These particles were catalytically inactive: no nanotube growth was observed with SOC0.05 and only sparse growth was observed with SOC0.5. Increasing the concentration of iron nitrate to 4.0 mg/mL (Figure 1c−e) increased particle size as well as the number and diameter of the carbon nanotubes formed. The nanotubes from SOC0.5 and SOC4 appear to grow along or subsequently rest on the silicon oxide surface. For the

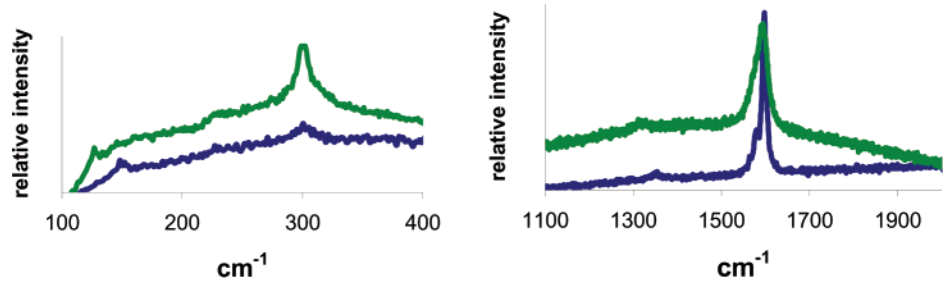


**Figure 2.** Representative microRaman spectra at 514 nm (blue, bottom) and 633 nm (green, top) of SOC4-produced carbon nanotubes.

intermediate iron nitrate concentrations, catalyst particles (~5−14 nm) were substantially larger than the diameter of the nanotubes (1−2 nm). The mean nanotube diameter is consistent with the formation of single-wall nanotubes. The SEM image of Figure 1d obtained from an intermediate iron nitrate concentration demonstrates the typical network of SWNTs formed and the high contrast spots that are presumed to be catalyst or potential catalyst particles. Concentrations of iron nitrate between 4 and 9 mg/mL (data not shown) resulted in an increased surface density of nanotubes as well as increased nanotube bundling. At higher concentrations (>10 mg/mL of iron nitrate; Figure 1f), larger particles (~18 nm) and nanotubes (mean diameter ~17 nm) were observed, consistent with the formation of predominately multiwall nanotubes. The average catalyst size is approximately the same as the apparent tube diameter.

Raman spectroscopy provided verification that the nanotubes observed at intermediate iron nitrate concentrations were single wall.[10] Typical spectra obtained by micro-Raman at 514 and 633 nm on SOC4 grown nanotubes are shown in Figure 2. The portion of the spectra between 400 and 1100 $cm^{-1}$ was omitted for clarity. This region contains resonances from the substrate ($Si/SiO_2$), which are orders of magnitude greater in intensity than the SWNT peaks of interest. The G peak, ~1600 $cm^{-1}$, is associated with the optical mode $E_{2g}$ of graphite and is characteristic of $sp^2$ hybridized carbon materials. The line shape of the G peak is thought to be dependent upon the metallic or semiconductor nature of the nanotubes present. The broader peak observed in the 633 nm spectrum is ascribed to metallic SWNTs. The smaller D peak at ~1300 $cm^{-1}$ reflects the level of disorder within the $sp^2$ carbon lattice. Qualitative information about the defect density of the nanotubes may be garnered from the intensity ratio of the D:G peaks. For the SOC4 nanotubes, values approaching zero indicated very low defect concentration. The radial breathing mode (RBM) regime (100−400 $cm^{-1}$) displayed the usual substrate-associated peak at 302 $cm^{-1}$ and peaks with a maximum at 152 $cm^{-1}$ ($\lambda$ = 514 nm) and 127 $cm^{-1}$ ($\lambda$ = 633 nm). The RBM of single-wall nanotubes is sensitive to diameter and excitation energy, enabling the diameter of nanotubes in resonance with a given laser wavelength to be calculated. For a collection of nanotubes with a distribution of diameters, only those nanotubes with the appropriate resonance conditions will be observed in the RBM region of the Raman spectra. Using the formula $\omega_{RBM} = \alpha/d$, where $\omega$ is the shift of the RBM peak with respect to the major silicon peak at 521 $cm^{-1}$ and $\alpha$ is a constant determined by the substrate (248 nm/cm for $Si/SiO_x$),[10] the diameter, $d$, can be determined. The observed RBM peaks correspond to single-wall nanotube diameters of 1.63 nm ($\lambda$ = 514 nm) and 1.96 nm ($\lambda$ = 633 nm). These values are in close agreement with the AFM data (1.88 nm for SOC4).

Further confirmation of single-wall nanotube structures was obtained through high-resolution transmission electron microscopy (HRTEM). An HRTEM image of an area similar to that shown in Figure 1c is displayed in Figure 3. As can be seen in the image, two single-wall nanotubes protrude from the edge of the $SiO_x$ matrix and reenter at a later point (arrows). The approximate diameters of these tubes were 1.3 and 1.7 nm—consistent with the AFM and Raman data. Furthermore, a root growth model is suggested by the observations of metal particles imbedded in the $SiO_x$ matrix from which nanotubes are extending outward (highlighted by the dashed circle and line).

To demonstrate the ability to create three-dimensional forms from the catalyst−preceramic polymer system, fibers were pulled from viscous solutions of SOC4 and then subjected to growth conditions described previously. Figure 4a is a low-magnification SEM image of the resultant ceramic $SiO_x$ fiber. Higher magnification images (Figure 4b) reveal nanotubes wrapped around the $SiO_x$ fibril.

Surface resistivity of two nanotube-coated $SiO_x/Si$ substrates were 300 $k\Omega/\square$, as determined by a 4-point probe method. Calculation of the surface conductivity directly from the geometric dimensions of the sample without accounting for nanotube surface density (void regions) yielded a value of 30 S/cm. Assuming the nanotubes occupy 10% of the surface area, a conservative estimate based on microscopy, then the conductivity of the nanotube network is estimated to be closer to 300 S/cm. Comparable measurements of the analogous, annealed catalyst-imbedded $SiO_x$ film before nanotube growth and the $SiO_x$ layer obtained from Accu-glass T1-11 had resistance values out of the range of the instrumentation (i.e., $>10^9$ k$\Omega$). The surface conductivities of the nanotube-coated $SiO_x$ are substantially greater than necessary for electrostatic discharge coatings ($10^2$−$10^9$ k$\Omega/\square$) and approaching the regime required for electromagnetic shielding applications ($<10^2$ k$\Omega/\square$).[11] Additionally, because the surface is optically

(10) Dresselhaus, M. S.; Dresselhaus, G.; Jorio, A.; Souza Filho, A. G.; Saito, R. *Carbon* **2002**, 2043−2061.

(11) Andrews, R.; Jacques, D.; Qian, D.; Rantell, T. *Acc. Chem. Res.* **2002,** *35*, 1008−1017.

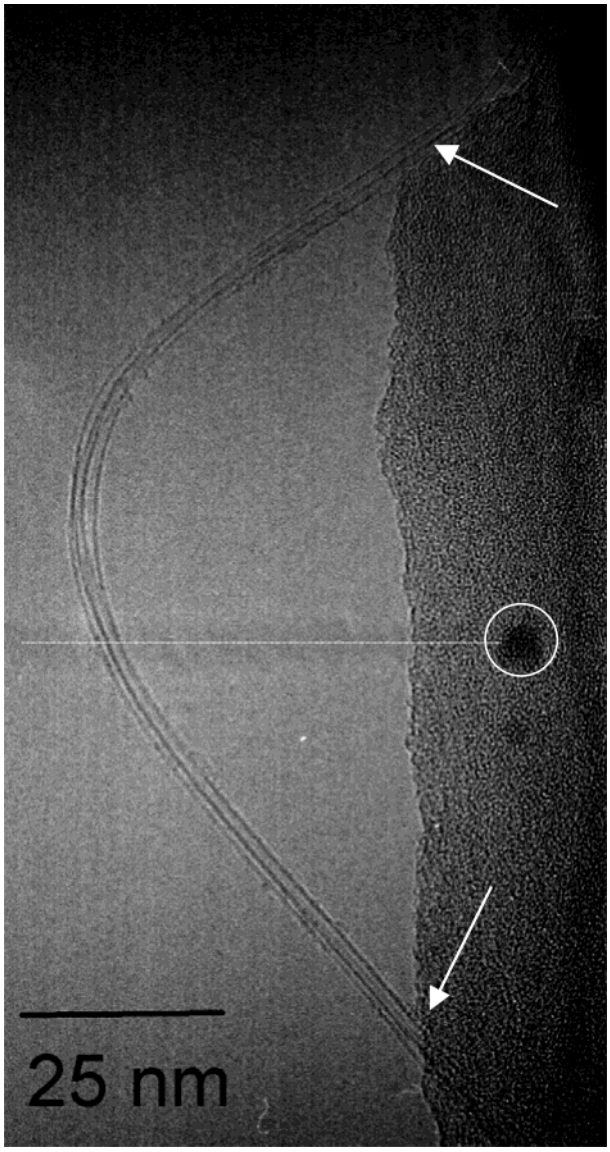


**Figure 3.** HRTEM image of two nanotubes extending from an SOC4-coated gold TEM grid. Arrows indicate the tube−matrix interface. Dashed line indicates an out-of-focus catalyst particle and nanotube.

transparent after growth (quartz substrates remained clear) the spin-on catalyst route may enable transparent electrodes (e.g., commercially available (CERAC) ITO at $>10^2$ kΩ/□ has only 90% transmission).

## Discussion

In the simple formulations of spin-on catalyst, the iron nitrate dissolves in the acetone/alcohol solvent phase of the spin-on glass. Upon solvent evaporation, phase separation between the largely immiscible salt and methylsiloxane polymer is anticipated to produce iron nitrate particles at the polymer−air interface. Subsequent thermal treatment converts the methylsiloxane polymer to $SiO_x$, and is anticipated to also produce iron particles (following in situ reduction in the $CH_4/H_2$ environment), which are subsequently available to catalyze the growth of carbon nanotubes.

The concentration of the salt in the initial solution affects the final size of the catalytic particles; SOC0.05 and SOC0.5 had roughly the same diameter, whereas SOC4 and SOC10 had particles three to four times larger. Interestingly, particles with an average diameter of 15 nm still led to the formation of SWNTs. This is in sharp contrast to the general consensus linking catalyst particle diameter directly to the resulting nanotube diameter. Because the formation of $SiO_x$ from the methylsiloxane polymer precursor occurs at temperatures below that of tube growth, the ceramic matrix will substantially reduce agglomeration of the metal particles, and therefore the size of the catalyst particles is expected to be determined before tube growth begins. Nevertheless, the final particle size is substantially greater than the diameter of the SWNTs formed.

Reactions during the thermal treatment between the as-formed $SiO_x$ (or an intermediate) and $Fe^{3+}$ may lead to the formation of catalytically inactive iron silicide before the system reaches nanotube growth conditions. Previous reports have established the formation of iron silicide at comparable temperature regimes for iron films sputtered on silicon substrates.[12] These iron compounds proved to be much less reactive than iron on other substrates (TiN or $Si_3N_4$) toward the catalysis of carbon nanotube growth.

For the SOC system, HRTEM and X-ray diffraction studies proved inconclusive to enable compositional characterization of the catalyst particles as the particles were not of sufficient crystallinity or concentration. Initial X-ray photoelectron spectroscopy (XPS) studies on a sample of a typical SOC-coated substrate (Figure 5) indicate a shift of the Fe $sp^2$ of iron (III) nitrate (712 eV) in the as-cast SOC film to lower binding energies (708 eV) upon heating to 900 °C in an inert atmosphere. Qualitatively similar XPS spectra have been reported for the formation of iron silicide from iron films sputtered on silicon wafers.[12a] However, the broadness of the peak observed would seem to indicate the presence of multiple iron species, which have yet to be identified.

Consistent with these initial observations, we speculate that the particles observed via microscopy are compositionally complex with only a minor volume fraction of iron that may be activated to catalyze SWNT growth under these conditions. Iron nitrate particle formation occurs initially via phase separation, followed at higher temperatures and later times by an interfacial, diffusion-limited reaction converting the iron nitrate to iron silicide. Within the time scale of the experiments, larger particles may not be completely converted to the silicide. Defects and surface cracks enable iron species within the core, which have not formed silicide, to be reduced to $Fe^0$ and catalyze the growth of SWNTs. Lower iron nitrate concentrations result in smaller particles, which are overwhelmed by the formation of silicide before conditions are favorable for carbon nanotube growth. Greater iron nitrate concentrations and the associated larger particles would result in incomplete conversion and the retention of reactive catalytic sites associated with the largest iron particles. Such

(12) (a) de los Acros, T.; Vonau, F.; Garnier, M. G.; Thommen, V.; Boyen, H. G.; Oelhafen, P.; Düggelin, M.; Mathis, D.; Guggenheim, R. *Appl. Phys. Lett.* **2002**, *80* (13), 2383−2385. (b) Wan, Q.; Wang, T. H.; Lin, C. L. *Chin. Phys. Lett.* **2003**, *20* (2), 301−303. (c) Jung, Y. J.; Wei, B.; Vajtai, R.; Ajayan, P. M.; Homma, Y.; Prabhakaran, K.; Ogino, T. *Nano Lett.* **2003**, *3* (4), 561−564. (d) Homma, Y.; Kobayashi, Y.; Ogino, T.; Takagi, D.; Ito, R.; Jung, Y. J.; Ajayan, P. M. *J. Phys. Chem. B* **2003**, *107*, 12161−12164.

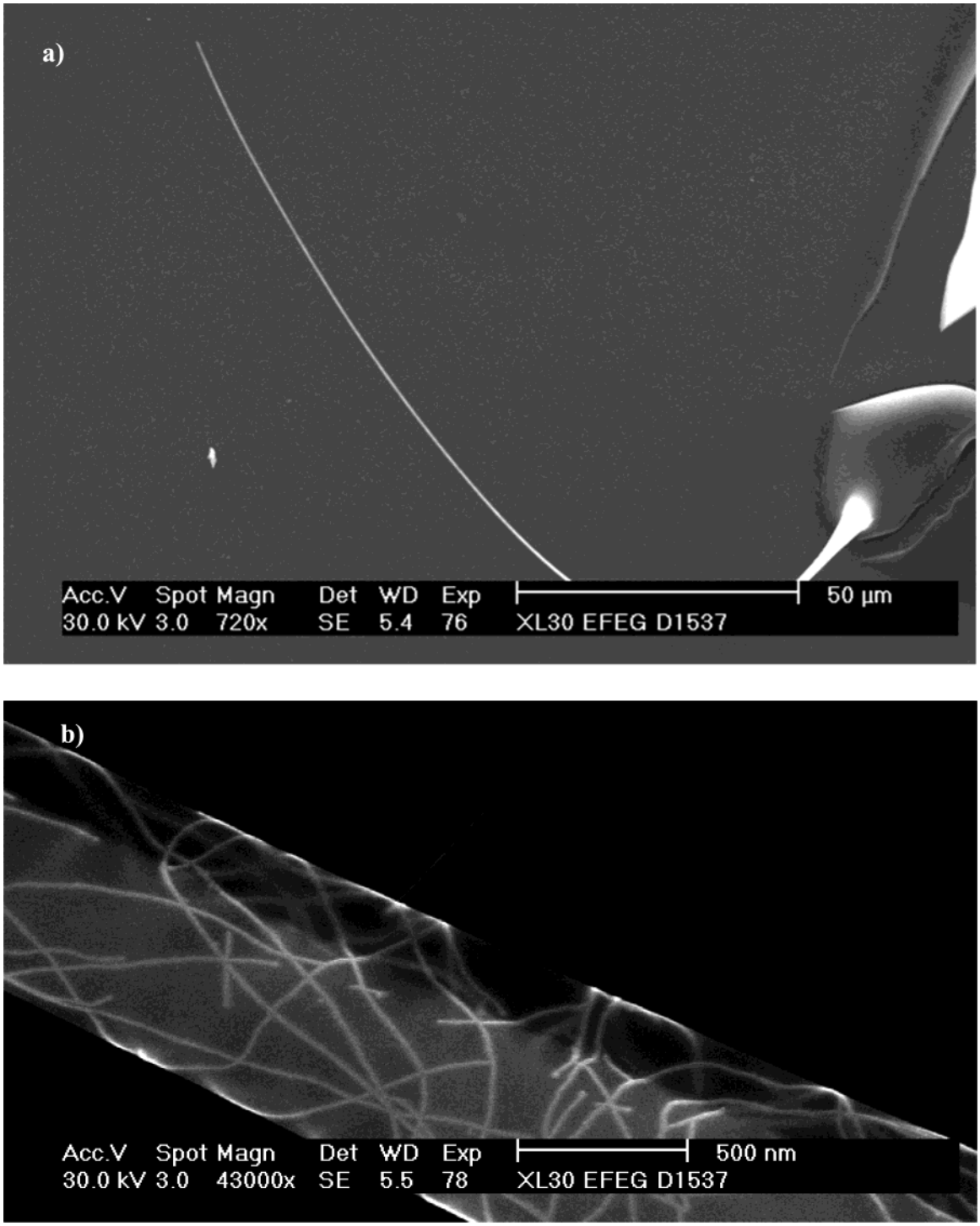


**Figure 4.** (a) Low-magnification SEM image of fiber pulled from viscous SOC4. (b) Higher -magnification SEM image of SOC4 fiber after nanotube growth.

occurrences would explain why only a minor fraction of the particles on the SOC0.5 substrate initiated growth, even though all the particles were of sufficient size to initiate growth if they consisted wholly of iron.

To prevent the formation of iron silicide, an SOC4 coated substrate was heated to 900 °C in flowing air to ensure the formation of iron oxide particles. Using the same growth conditions that yielded SWNTs from the unoxidized SOC4 (Figure 1d), the oxidized substrate yielded multiwall nanotubes with diameters of ~10−20 nm or the size range of particles observed in the AFM study. The initial formation of the iron oxide enabled the majority of the iron atoms present on the surface to, under the reducing growth conditions, form $Fe^0$ and subsequently catalyze the growth of observed structures.

The initial phase separation between the salt and the polymer host dictates the formation of discrete particles; the size scale of which is dictated by the $Fe(NO_3)_3$ concentration. At some point during the thermal treatment in an inert atmosphere, the iron nitrate reacts with its matrix host and forms a compositionally complex system partially similar to an iron silicide. Considering first that iron silicide has been shown to be inactive for the catalysis of SWNT growth and,

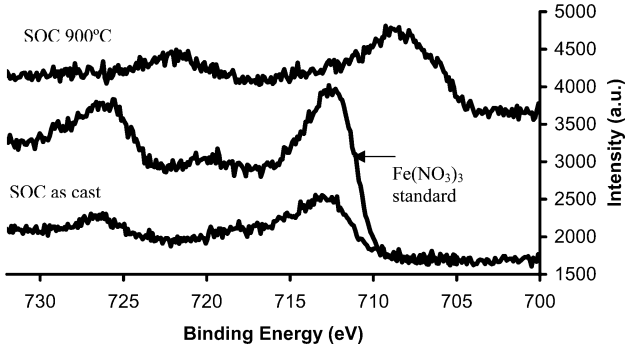


**Figure 5.** XPS spectra of iron nitrate standard (middle), SOC as-cast (bottom), and SOC heated to 900 °C in argon.

second, that preferential formation of iron oxide from the same size scale particles leads to multiwall nanotube growth, the remaining iron species in the SOC system must be of sufficient volume and must be sufficiently reducible to catalyze the growth of SWNTs as observed. Further experiments are underway to probe and more fully characterize the reaction of iron with the matrix within the SOC systems under nanotube growth conditions and the impact of the particles formed on the observed nanotube products.

## Conclusion

In summary, the spin-on catalyst system provides a flexible and simple approach for the synthesis of single-wall carbon nanotubes. Formation of discrete nanotubes was observed at iron nitrate concentrations between 0.5 and 10 mg/mL in spin-on-glass. Raman spectra indicated that limited defects were present in the nanotubes and along with TEM, no evidence for amorphous carbon deposition was observed. Furthermore, the number of tubes per unit area as well as the effective particle size of the catalyst can be controlled easily by varying the concentration of the iron salt in the preceramic polymer. The simultaneous conversion of the precermaic polymer to $SiO_x$, in-situ formation of catalyst particles and nanotube growth utilizing the same processing temperatures and environment simplifies fabrication protocols. Additionally, the initial understanding of catalyst formation broadens the potential role of the preceramic polymer beyond inhibition of catalyst coarsening at tube growth temperatures to chemically participating in the in-situ formation of structurally complex catalyst particles.

The catalyst−preceramic polymer system is useful on various substrates, including those discussed above as well as on quartz and graphite (not shown), is easily patterned (work in progress), and allows for the formation of unique glassy, SWNT-coated, three-dimensional structures. As mentioned, this flexibility could lead to replacements for traditional materials and components in electrostatic discharge, electromagnetic shielding, and transparent electrode applications. Finally, because spin-on-glass is an established component in microelectronic fabrication processes, the SOC system provides a platform for facile integration with current processes, facilitating the incorporation and development of single-wall-nanotube-based microelectronic structures.

**Acknowledgment.** We gratefully acknowledge the National Research Council (NRC) and the Air Force Office of Scientific Research (AFOSR) for funding this work, Dr. Robert Wheeler for HRTEM, Dr. John Ferguson for electrical measurements, and Applied Sciences, Inc. for temporary furnace use. Additional thanks to Dr. Emmanuel Gianellis of Cornell University for RBS characterization and Dr. Jeffrey Sanders and Benjamin Phillips for XPS characterization.

CM034851S